Magnetic susceptibility and specific heat of a spinel MnV_2O_4 single crystal

Kim Myung-Whun,[1,2] J. S. Kim,[1,3] T. Katsufuji,[4] and R. K. Kremer[1]

[1]*Max-Planck-Institut für Festkörperforschung, Heisenbergstraβe 1, D-70569 Stuttgart, Germany*

[2]*Institute of Photonics and Information Technology, Chonbuk National University, Jeonju 561-756, Korea*

[3]*Department of Physics, Pohang University of Science and Technology, Pohang, Korea*

[4]*Department of Physics, Waseda University, Tokyo 169-8555, Japan*

(Received 28 February 2010; revised manuscript received 5 November 2010; published 19 January 2011)

We investigated the magnetic and the thermodynamic properties of a spinel MnV_2O_4 single crystal. The magnetization and susceptibility show the signature of ferromagnetic ordering at ~61 K. A sharp peak in the magnetization and the specific heat indicate the structural phase transition at 58 K, consistent with the scattering experiments. The specific-heat data exhibits the signature of double transitions. In addition to the higher-temperature transition at T_S, the second transition occurs at a lower temperature T^*, which divides the phase below T_S into a low-magnetic-field and a high-magnetic-field phase. Based on the magnetic susceptibility and the specific heat, a wide-range temperature and magnetic-field phase diagram was constructed. The low-magnetic-field phase shows the characteristics of a spin-glass-like state. A comparison with the magnetic and thermodynamic characteristics of similar materials suggests that the low temperature and low-magnetic-field, spin-glass-like phase in MnV_2O_4 may originate from the competition between the interchain and the intrachain exchange interaction owing to the fluctuating V-ion orbitals.

DOI: 10.1103/PhysRevB.83.024403 PACS number(s): 75.30.Cr, 75.40.Cx, 76.30.−v, 76.50.+g

I. INTRODUCTION

MnV_2O_4 is a spinel ferrimagnet. Mn^{2+} ($3d^5$) ions occupy the tetrahedral sites and V^{3+} ($3d^2$) ions occupy the octahedral sites. This compound has been studied owing to the collinear-to-noncollinear magnetic-phase transition accompanied by a cubic-to-tetragonal structural transition.[1,2] Recently, it has attracted renewed attention because of the intriguing magnetic ground state in spinel transition-metal oxides as well as the multiferroic properties observed in the related spinel structures.[3–5] Understanding the underlying mechanism for those intriguing phenomena, however, is difficult because of the complicated interplay between the lattice, spin, and orbital degrees of freedom.

In the spinel lattice of MnV_2O_4, both the Mn ions and the V ions form a geometrically frustrated network. The basic coordination element of Mn ions is a triangle because the Mn-ion sublattice forms a diamond structure.[6] The V ions form the chains that run along the (110) (or xy), (101) (xz), and (011) (yz) directions of the original cubic structure.[5] The chains interfere with each other by forming a triangular network.

The spin structure is prone to enhance the geometrical frustration. The Mn spins have a large magnetic moment while the V spins have a small magnetic moment. However, the strength of the magnetic interaction is relatively weak for the Mn spins because the exchange path between two Mn ions involves at least three intermediate ions. Note that the Weiss temperature of the $MnAl_2O_4$ is 140 K.[6] On the other hand, the interaction between the V spins is relatively strong because the exchange path between the two V ions is shorter than that of Mn ions. The high Weiss temperature of ZnV_2O_4 (≈1000 K) suggests a strong V-V interaction in the spinel structure.[7] The combination of large moment spins with weak exchange interaction and small moment spins with strong exchange interaction can give rise to a complicated magnetic ground state.

The partially filled t_{2g} orbitals of the V ion have been known to induce the complicated magnetic interactions as reported for ZnV_2O_4.[8] Some theoretical calculations suggest that the orbital selective electron occupancy results in a bond-dependent exchange interaction frustrated on the spinel lattice of ZnV_2O_4.[9] The anti-Jahn-Teller-type VO_6 octahedral distortion lifts the orbital degeneracy and leads to the orbital ordering. However, the degenerate doublet might survive the orbital ordering, and the spins in the doublet can be involved in the spin-orbit coupling.[10] The competition between the orbital selective exchange interaction, the Jahn-Teller distortion, and the spin-orbit coupling may drive the system into a strongly frustrated ground state.

MnV_2O_4 is a rare example where the frustrated interactions between the spin, orbital, and lattice are active and all intermingled. An examination of the magnetic-field dependence of the susceptibility and the specific heat of MnV_2O_4 will give some insights into the spin and orbital ground-state characteristics of V sites under the strong and complicated frustrated interaction.

The physical properties, including the magnetic susceptibility and the specific heat of MnV_2O_4, have been reported already,[2,3,11–13] however, some properties such as the transition temperature, the shape of the magnetic susceptibility, and the neutron-diffraction curve are found to be quite sensitive on the sample quality.[1,3,13,14] The reason is unclear, but the imperfections, such as the grain boundaries, may cause differences in the physical properties.[3,12,13] Therefore, a study of a single crystal is in demand; however, the currently available study of the single crystal is focused on the small temperature and magnetic-field range.[12,13] This paper reports the dc and ac magnetic susceptibility and the specific heat of a MnV_2O_4 single crystal in a wide-temperature and magnetic-field range. This study focuses on the temperature and external magnetic-field dependence of the phase transition at temperatures lower than the structural phase-transition temperature in an attempt to explain the origin of the phase transition in terms of the

competition between the bond selective exchange interactions owing to the orbital fluctuations on the spinel lattice.

II. EXPERIMENT

A MnV_2O_4 single crystal was grown by a floating-zone method. The crystal structure was characterized by x-ray diffraction, as described in detail elsewhere.[13] The dc and ac magnetic susceptibilities were measured by using a upercon-ducting quantum interference device (SQUID) magnetometer (MPMS). For the ac susceptibility, a driving field of 1 Oe was applied over the frequency range of 0.02 Hz to 1 kHz. The specific heat (C_P) was measured by using a physical property measurement system employing the relaxation method. A minute amount of Apiezon N grease was used to thermally anchor the crystals to the sapphire sample platform. The specific heat of the platform and grease was determined in a separate run and subtracted from the measurements of the sample. Two different magnitudes of heat pulses generating $\Delta T/T \approx 1\%$ and 0.3% were used to check for possible extrinsic error near the first-order transition. In both cases, similar C_P anomaly and transition temperatures were obtained. For the C_P measurements under external magnetic fields, the sample was cooled slowly after applying the magnetic field along the (001) direction of the single crystal at room temperature.

III. RESULTS

A. Magnetic susceptibility

The magnetic susceptibility of MnV_2O_4 shows the ferromagnetic temperature dependence with a few anomalies. Figure 1(a) shows the temperature (T) dependence of the magnetization [$M(T)$] curve from 300 to 2 K. The $M(T)$ curve increases rapidly with decreasing temperature below ~65 K, indicating a spontaneous ferromagnetic ordering. The $M(T)$ curve shows a peak near 50 K, and the $M(T)$ decreases drastically with decreasing temperature for the zero-field-cooled (ZFC) run. The $M(T)$ of the field-cooled (FC) run also decreases but it increases again below ~40 K. The breakaway between the ZFC and FC runs begins at 55 K [see the inset of Fig. 1(a)] and becomes significant below ~40 K. Those observations are qualitatively consistent with previous studies[2,3,11,12]

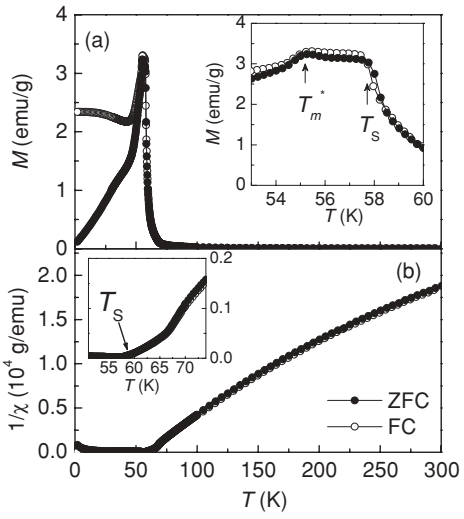

FIG. 1. (a) Temperature dependence of the magnetization [$M(T)$] of ZFC (solid circle) and FC (open circle). In the inset, the $M(T)$ curve near 60 K was magnified. Here the phase-transition temperatures, T_S and T_m^* (see the text for the definition), are indicated by the arrows. (b) Inverse susceptibility [$1/\chi(T)$] at $H = 100$ Oe. The dotted line is a guide to the eye for the high-temperature linear part. The inset shows the $1/\chi(T)$ curve near T_S.

The inverse of the magnetic susceptibility [$1/\chi(T)$] shows the signature of the magnetic ordering more clearly, as shown in Fig. 1(b). With lowering temperature from 300 K, the $1/\chi(T)$ decreases and its slope remains almost linear until ~200 K. Below 200 K the curve deviates from the high-temperature linear slope, which is often observed in ferrimagnetic materials. The inset of Fig. 1(b) magnifies the $1/\chi(T)$ at ~60 K. The $1/\chi(T)$ approaches the zero value of the ordinate, as usually seen in ferromagnetic materials. It has been reported that the ferrimagnetic collinear spin ordering develops at ~61 K by a recent neutron-scattering experiment.[14]

The linear extrapolation of the $1/\chi(T)$ as a usual conduct does not yield the convincing identification of the ferrimagnetic ordering temperature T_C, owing to the nonlinear curvature. The Arrott plot was drawn in Fig. 2 to estimate the T_C more accurately. Figure 2(a) shows the $M^{1/\beta}$ vs $(H/M)^{1/\gamma}$ plot ($\gamma = 1$ and $\beta = 0.5$). The plots below 58 K show the typical shape with a high magnetic-field linear slope, the plots above 63 K show the nonlinear shape, and the plots between 60 and 63 K show the *S*-like curvature change in the intermediate-magnetic-field range. The nonlinear shape of the plots could be owing to the spin fluctuation, disorder, or the contribution of the higher-order magnetization.[15,16] To get a better estimation, the modified Arrott plot, i.e., $M^{1/\beta}$ vs $(H/M)^{1/\gamma}$ ($\gamma = 1.4$ and $\beta = 0.39$), was drawn in Fig. 2(b). The plots between 60 and 63 K still show the nonlinear curvature, and owing to the nonlinear curvature, the T_C cannot be identified clearly from the linear extrapolation of the plots.

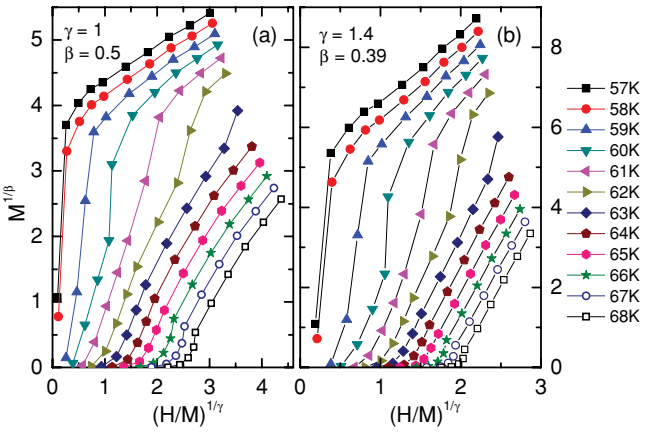

FIG. 2. (Color online) Arrott plot isotherms, $M^{1/\beta}$ vs $(H/M)^{1/\gamma}$, near 60 K. (a) The conventional Arrott plot ($\gamma = 1$ and $\beta = 0.5$) and (b) the modified Arrott plot ($\gamma = 1.4$ and $\beta = 0.39$) are shown. The unit of M is μ_B and the unit of H is T.

However, the ordinate value of the linear extrapolation of the high-magnetic-field data crosses zero between 61 and 62 K, which suggests that the ferrimagnetic ordering temperature T_C is ~61 K, consistent with the neutron-scattering experiment.[14]

In addition to the ferromagnetic transition, there are two subsequent phase transitions. The inset of Fig. 1(a) magnifies the peak region of the $M(T)$ curve just below T_C. Two cusps in $M(T)$ appear at 58 and 55 K. The first cusp appears at 58 K, which corresponds to the onset temperature of the noncollinear triangular spin ordering observed in the neutron-scattering experiment.[14] X-ray and neutron-diffraction experiments reported a change in the lattice structure from a cubic to a tetragonal lattice at this temperature.[13,14] We define this temperature as T_S.

The second cusp appears at 55 K, corresponding to the onset temperature of the breakaway between the ZFC and the FC runs of the $M(T)$ curves. No signature of the spin or the lattice transition was detected in neutron-scattering or x-ray scattering experiments at this temperature. The breakaway behavior often appears in the spin-glass materials,[17,18] disordered alloy magnets,[17,19] or frustrated magnets such as $Y_2Mo_2O_7$.[20–22] A similar breakaway and the suppression of $M(T)$ were also observed in spinel magnets such as $MnCr_2O_4$ and $CoCr_2O_4$; for those compounds the origin has been attributed to the formation of spin-glass clusters.[23] We define this temperature as T_m^*. In a previous study, it was defined as the orbital-ordering temperature.[12]

The ac susceptibility, $\chi(f,T)$, at zero magnetic field shows significant frequency (f) dependence, suggesting the formation of the spin-glass-like phase at low temperature. Figure 3(a) shows the real part, $\chi'(f,T)$, and Fig. 3(b) shows the imaginary part, $\chi''(f,T)$, at different frequencies ranging from 0.02 Hz to 1 kHz. The $\chi'(f,T)$ and $\chi''(f,T)$ have a similar temperature dependence with dc susceptibility even at 1 kHz, and both exhibit a weak frequency dependence similar to some ferro- or ferrimagnets.[25]

The $\chi'(f,T)$ shows negligible frequency dependence above T_m^*, but a move in the susceptibility curve to higher temperature as the frequency increases below T_m^*. Such an effect is more significant between 30 and 45 K. We defined the largest inflection point on the $\chi'(f,T)$ curve at a given frequency as the inflection temperature, T_i, to estimate the frequency-dependent shift of the susceptibility. The inset of Fig. 3(a) shows the T_i of several frequencies on a logarithmic scale. T_i increases from 38.2 K at 0.02 Hz to 40.5 K at 1 kHz as f increases. A similar frequency dependence has been observed in some amorphous materials and disordered alloys where some spin-glass state is formed.[18,24,26,27] The empirical Vogel-Fulcher curve denoted as the solid line fits the observed T_i values quite well. The $\Delta T_i/[T_i \log_{10}(f)]$ obtained from the fit is 0.015, comparable to those of spin-glass materials,[27] and consistent with a previous study.[29]

The $\chi''(f,T)$ shown in Fig. 3(b) is qualitatively similar to $\chi''(f,T)$. It also shows a pronounced frequency dependence between 55 and 20 K with a maximal difference at ~35 K, as shown in the inset of Fig. 3(b). However, the $\chi''(f,T)$ value is ~10× smaller than that of $\chi'(f,T)$, and the suppression becomes more significant as the applied frequency increases. The frequency-dependent shift occurs not only below T_m^* but also above T_m^*.

Three phase transitions show different magnetic-field dependences. Figure 3(a) shows the $M(T)$ curve for the warming run (solid circle) and the cooling run (open circle) at various magnetic fields. Although we cannot trace the magnetic-field dependence of T_C clearly in the $M(T)$ curve, T_S exhibits an apparent increasing behavior with magnetic fields. Two arrows on the $M(T)$ curve in Fig. 4(a) correspond to the T_S of the warming run and the cooling run for 0.1 T, respectively, indicating a thermal hysteresis. Figure 4(b) summarizes the magnetic-field dependence of T_S. The T_S's of the warming run and the cooling run commonly increase as the magnetic field increases. The slope of the increase is almost linear, but the slope changes at ~3 T. The width of the hysteresis

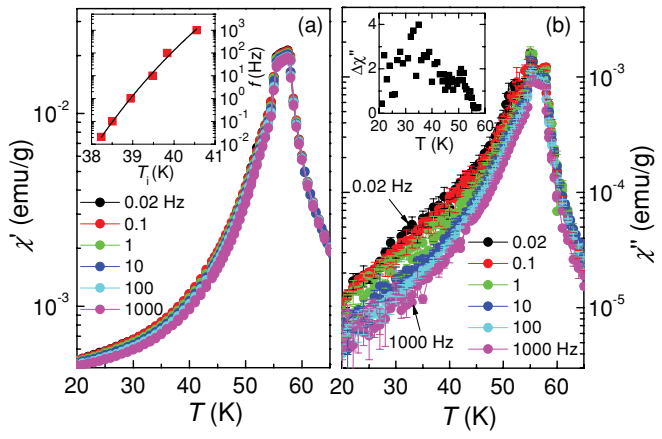

FIG. 3. (Color online) Temperature dependence of (a) the real part of ac susceptibility with an ac magnetic field of $H_{ac} = 1$ Oe and various frequencies, f. In the inset, the frequency dependence of the inflection point of the real part of the ac susceptibility is presented. The (red) solid line is the best fit of the Vogel-Fulcher law. (b) The imaginary part of the ac susceptibility. In the inset, $[\chi''(0.02\ \text{Hz},T) - \chi(1000\ \text{Hz},T)]/\chi(1000\ \text{Hz},T)$ was shown.

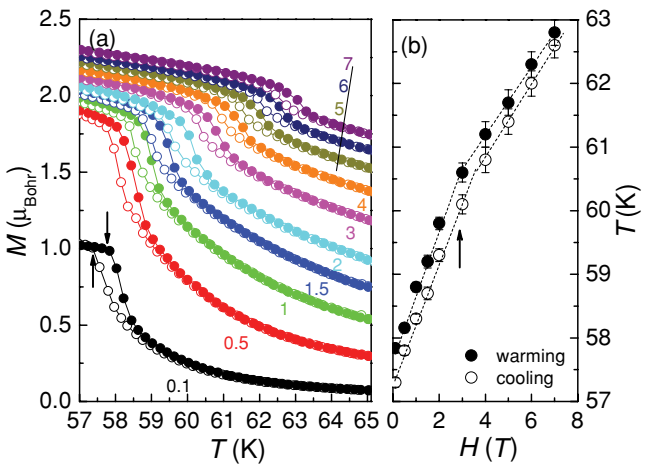

FIG. 4. (Color online) (a) Magnetization (M) near the phase-transition temperature, T_S, under various magnetic fields. (b) Magnetic-field dependence of T_S. The solid (open) symbols correspond to the data taken during the warming (cooling) run.

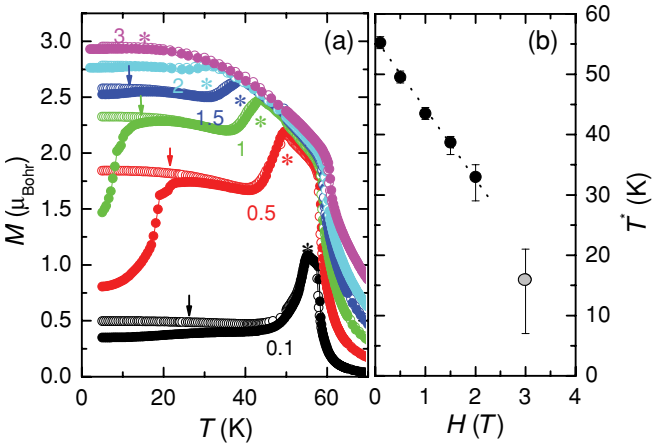

FIG. 5. (Color online) (a) Magnetization (M) near the phase-transition temperature, T_m^*, with various magnetic fields. The solid (open) symbols correspond to the data taken during the ZFC (FC) run. (b) Magnetic-field dependence of T_m^*.

temperature region remains relatively constant (∼0.5 K) for all of the magnetic field measured.

On the contrary, the transition at T_m^* is suppressed by the magnetic field (H). Figure 5(a) shows the $M(T)$ below 70 K as a function of the applied magnetic field from 0.1 to 3 T. The $M(T)$ curve shows the breakaway below T_m^* (denoted by the asterisks) as well as the suppression for the low field ($H < 3.0$ T), while it shows the typical ferromagnetic saturation at low temperatures above 3 T (not shown). The feature at T_m^* becomes weaker as the magnetic field increases without any noticeable thermal hysteresis, and it is obliterated

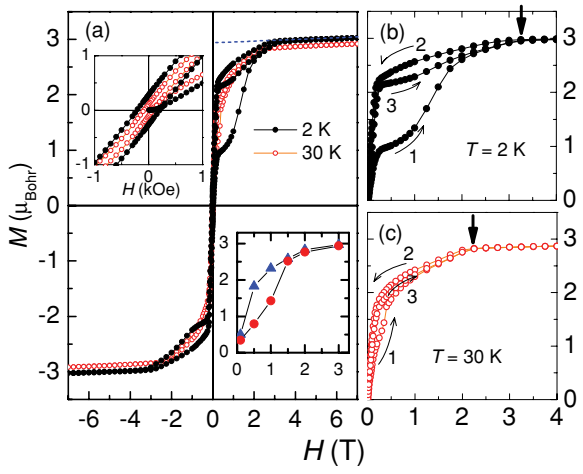

FIG. 6. (Color online) (a) Magnetic-field dependence of magnetization (M) at 2 and 30 K up to 7 T after full cycling ($0 \rightarrow 7$ T $\rightarrow 0 \rightarrow 7$ T $\rightarrow 0 \rightarrow 7$ T $\rightarrow 0$). In the upper-left-hand inset, the low-magnetic-field response up to 1 kOe is shown. In the lower-right-hand inset, the saturated magnetization at 5 K obtained in $M(T)$ is shown. The solid triangles in the inset correspond to the saturated magnetization of FC $M(T)$ and the solid circles correspond to the saturated magnetization of ZFC $M(T)$. (b) The first quadrant ($M > 0, H > 0$) $M(H)$ curve at 2 K; arrows represent the ramping order. The solid triangle marks the magnetic field where the bifurcation ends and the change in slope occurs. (c) The first quadrant $M(H)$ curve at 30 K.

at 3 T. The magnetic-field dependence of T_m^* is summarized in Fig. 5(b).

The behavior of the ZFC magnetization curve is another point to be noticed. As the temperature decreases, the ZFC curve splits from the FC one below T_m^*, abruptly descends, slightly ascends, and finally falls. On the other hand, the FC curve does not follow the same path as the ZFC curve. It also abruptly descends below T_m^*, but it keeps almost constant or it slightly ascends to very low temperature. Not only T_m^* but the temperature where the ZFC curve falls [denoted by the arrows in Fig. 5(a)] also decreases as the external magnetic field increases. The abrupt fall of the ZFC curve seems most significant below 30 K and between 0.5 and 1.0 T.

A similar magnetic state was observed in $MnCr_2O_4$. Tomiyasu, Fukunaga, and Suzuki have found that the onset temperature of the ZFC fall in the $M(T)$ curve of $MnCr_2O_4$ is close to the spin-spiral structure domain-formation temperature observed by the neutron-scattering experiment.[23] From the analogy, we suspect that a similar complicated spin state is formed in MnV_2O_4 below the ZFC fall temperature. However, further experimental investigations are desirable for more concrete understanding.

The isothermal magnetization, $M(H)$, is shown in Fig. 6. At 2 K, the $M(H)$ shows an S-like hysteresis loop and saturates above 3.3 T with a saturation magnetic moment of 2.9 μ_{Bohr}. As the field decreases to zero after saturation, the $M(H)$ reaches the remnant moment of 0.3 μ_{Bohr} and the coercive field is 0.03 T [see the inset in the upper-left-hand quadrant of Fig. 6(a)]. Figure 6(b) magnifies the first quadrant of the $M(H)$ curve at 2 K. The normal induction curve following arrow number 1 increases sharply up to $H = 0.2$ T, which is typical of ferromagnets. Above 0.2 T the curve appears to saturate, but it increases again with increasing field above 1 T. The inset in the lower-right-hand quadrant of Fig. 6(a) shows the magnetization values at 5 K obtained from the FC $M(T)$ curves (triangles) and from the ZFC $M(T)$ curves (circles), which shows that trace 1 of the $M(H)$ curve is related to the magnetic feature that causes the ZFC fall shown in Fig. 5(a).

Note that there is a bifurcation between curves 2 and 3. The bifurcation seems to be related to the T_m^* phase. The bifurcation begins at 0.2 T and the magnetization reaches 80% of the saturation value (2.2 μ_{Bohr}) at this field, and it ends at 3.3 T, as marked by a triangle. A similar behavior was still found at higher temperatures, e.g., at 30 K, although the coercive field, the remnant moment, and the saturation value become smaller [Fig. 6(c)]. The bifurcation becomes weaker also, which begins at 0.3 T and ends at 2.2 T. The temperature and magnetic-field dependence of the bifurcation point may coincide with the phase boundary line of Fig. 5(b). The possible origin of the bifurcation will be discussed below.

B. Specific heat

At T_m^* and at T_S the specific heat shows peaks, but with different shapes and magnetic-field dependence. Figure 7 shows the temperature dependence of the specific heat divided by the temperature [$C_P(T)/T$] at zero magnetic field. The solid (open) circle corresponds to the warming (cooling) run. As the temperature increases, $C_P(T)/T$ increases almost

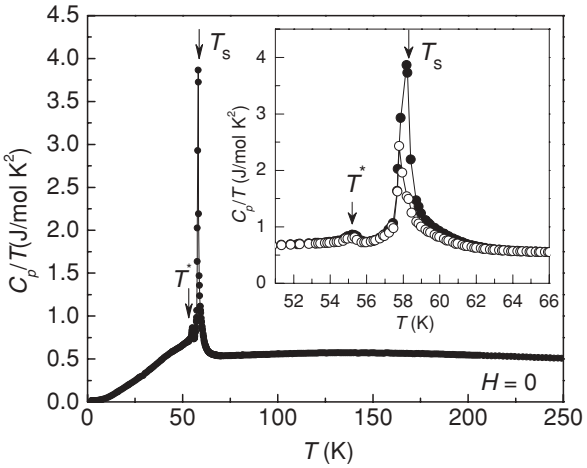

FIG. 7. $C_P(T)/T$ curve at $H = 0$ T. Inset: $C_P(T)/T$ curve measured during the warming (solid) and cooling (open) run. T_C, T_S, and T^* are indicated by the arrows.

linearly up to 50 K. A tiny peak appears at 55 K, where $M(T)$ shows significant breakaway (Fig. 1). This coincidence is observed for all the data measured under the magnetic field, which demonstrates that T_m^* indicates the phase transition. From now on we use T^* instead of T_m^*. At slightly higher temperatures, the $C_P(T)/T$ curve increases rapidly and shows a sharper and stronger peak at T_S. Above 70 K, the $C_P(T)/T$ increases very slowly and makes a very broad hump with a center at ∼150 K. Those observations are qualitatively consistent with the previous studies.

The inset of Fig. 7 shows that the hysteresis appears between 58 and 62 K. Because we employed a relaxation method for the $C_P(T)/T$ measurements, each data point was measured while the temperature was increasing with a small amount of the heat pulse after initially stabilizing the temperature. For the cooling sequence, the temperature decreased first and then increased slightly during the $C_P(T)/T$ measurements. In the case of first-order transition, the release of latent heat at the phase transition was fully captured only during the warming sequence of the measurements. Therefore, the significant $C_P(T)/T$ difference between the cooling and warming curve at T_S clearly indicates the first-order transition. However, the thermal hysteresis is almost absent near the small peak at T^*. Therefore, the transition at T^* may not be a first-order transition.

The $C_P(T)/T$ peak shows the large magnetic-field dependence near T_S. Figure 8(a) shows $C_P(T)/T$ under 0 T (circles) and $C_P(T)/T$ under 9 T (triangles). The sharp peak at T_S moves to a higher temperature by the magnetic field. Figure 8(b) magnifies the field dependence at T_S. The peak is at 58 K under 0 T and it moves up to 63 K as the magnetic field increases. The peak temperature rapidly increases from 0 to ∼3 T, while the increasing rate becomes relatively smaller above ∼3 T. Thus the slope of the increase changes ∼3 T. The slope change indicates the nonmonotonic magnetic-field dependence of T_S, which is consistent with the data obtained from $M(T_S, H)$, as shown in Fig. 4.

In contrast to the peak at T_S, the small peak at T^* moves drastically to lower temperatures with increasing magnetic field. As shown in Fig. 8(c), the peak at 55 K under 0 T

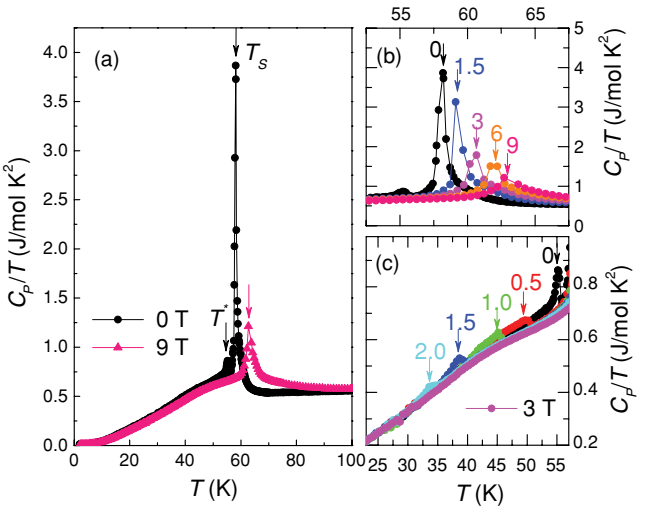

FIG. 8. (Color online) (a) $C_P(T)/T$ curves at $H = 0$ and 9 T. All data were obtained during warming after the FC run under magnetic field applied at room temperature along the (001) direction of the cubic-phase crystal. The phase-transition temperatures, T_S and T^*, are indicated by arrows. Note that the small anomaly at T^* is absent at $H = 9$ T. The $C_P(T)/T$ curves were shown near the phase transitions at (b) T_S and (c) T^* under various magnetic fields. The numbers next to the data correspond to the applied H field. The unit of the magnetic field is T.

moves to 33 K under 2.0 T. The anomaly becomes weaker at higher magnetic fields, and eventually it becomes invisible at high magnetic fields above 3 T. The dependence of the peak temperature is also consistent with the magnetic-field dependence of the T_m^* in the $M(T_m^*, H)$ curve shown in Fig. 5.

Figure 9 shows the specific heat at low temperatures. For a conventional ferrimagnet, its temperature dependence of the specific heat can be well described by the superposition of a T^3 term from phonons and a $T^{3/2}$ term from magnons. The $C_P(T)/T^{3/2}$ vs $T^{3/2}$ curve is expected to be a straight line at low temperatures, and its slope provides an estimate of the Debye temperature (Θ_D).[28] However, as shown in Fig. 9(a),

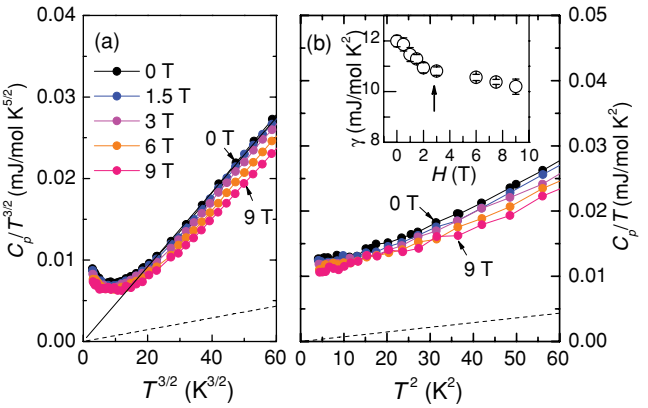

FIG. 9. (Color online) (a) $C_P/T^{3/2}$ vs $T^{3/2}$ and (b) C_P/T vs T^2 at different magnetic fields. The dashed lines represent the lattice specific heat of the Debye temperature, $\Theta_D = 300$ K. All data were obtained during warming after FC. Inset: The linear temperature contribution to C_P, i.e., γ as a function of magnetic field.

our data do not follow the linear dependence. Normally such a linear dependence of C_P to $T^{3/2}$ should become more pronounced as the temperature lowers and the lattice contribution to the C_P follows the Debye law. However, for MnV_2O_4 the deviation becomes even larger as the temperature decreases. Furthermore, the slope is steeper than that expected from the typical phonon contribution, yielding a Debye temperature, $\Theta_D \sim 160$ K. Note that the Debye temperature of $MnAl_2O_4$, whose lattice structure is similar with that of MnV_2O_4, was estimated to 312 K.[6] If we estimate the lattice specific heat roughly with $\Theta_D = 300$ K under zero magnetic field, the estimated contribution is still less than 10% (the dashed line) of the total specific heat.

The $C_P(T)/T$ curve reveals a strong linear contribution to C_P of the order of 10 mJ/mol K^2, as shown in Fig. 9(b). The linear-T contribution cannot be attributed to a typical Sommerfeld coefficient for electrons, because MnV_2O_4 is a good insulator in the whole temperature range for the measurements. The other possible cause of the large γ value could be the magnetic contribution. The linear temperature dependence of C_P is known for the spin-glass system such as pyrochlore $Y_2M_2O_7$ (M = Mn, Mo) (Refs. 21 and 22) and (Eu,Sr)S,[24] which show strong magnetic fluctuations at low temperatures. In the spin-glass system, the low-energy magnetic excitations remain constant at low temperatures owing to the frustrated and degenerate nature of the ground states, which leads to the linear temperature dependence of C_P. This explanation is, in fact, consistent with the spin-glass behavior in the ac susceptibility. The inset of Fig. 9(b) presents the γ values at several magnetic fields. The value decreases as the magnetic field increases, but the slope changes at ~3 T, which indicates that the magnetic fluctuation strength is altered ~3 T.

Finally, the derivative of the specific heat $[dC_P(T)/dT]$ exhibits the signature of the ferromagnetic ordering temperature, T_C. As shown in Fig. 10(a), the $dC_P(T)/dT$ reveals a weak concave structure on the steep uprising curve owing to the sharp peak of C_P/T at T_S. The inflection points of the concave structure marked by arrows were determined as the T_C of the given magnetic field. The T_C estimated from the Arrott plot is not precisely matched with the value. The discrepancy, however, could be owing to the uncertainty of the estimation method. The magnetic-field dependence of T_C is summarized in Fig. 10(b). The T_C increases almost linearly as the magnetic field increases, which is similar to the magnetic-field dependence of T_S. The slope seems to change ~3 T.

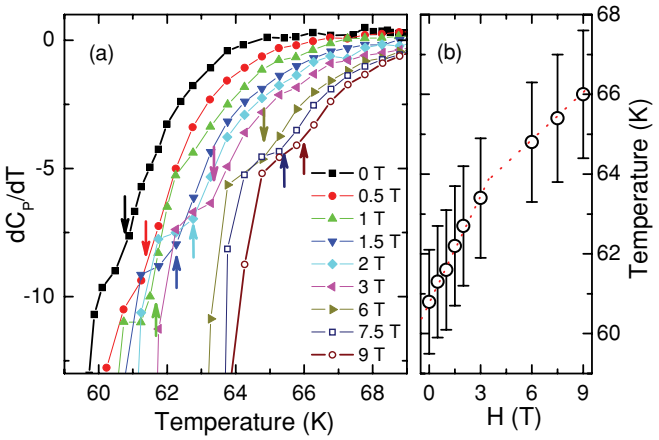

FIG. 10. (Color online) (a) The derivative of the specific heat, $dC_P(T)/dT$. The ferromagnetic ordering temperatures (T_C) are indicated by arrows. (b) The magnetic-field dependence of the T_C.

IV. DISCUSSION

Figure 11 summarizes the experimental results in the T-H phase diagram. It shows a qualitatively consistent diagram with the previous studies. At room temperature, the lattice is cubic and the magnetic state is paramagnetic (PM). As the temperature decreases, the system changes into a ferrimagnetic state. It is difficult to determine the ferrimagnetic ordering temperature, T_C, from the magnetic susceptibility and the specific heat precisely. Note that the error of T_C is quite large. This might be owing to the short-range magnetic ordering and its strong fluctuations up to a high temperature above T_C, as suggested in a neutron-scattering study.[1] The T_C appears to increase monotonically with increasing the magnetic field. A collinear antiparallel ordered state of Mn spins and V spins was observed just below T_C.[14]

Below T_C, there appears a clear boundary T_S, where the magnetic susceptibility and the specific heat change abruptly. The transition at T_S accompanies the thermal hysteresis in the magnetic susceptibility and the specific heat, which is consistent with the scattering experiments.[13,14] Below T_S,

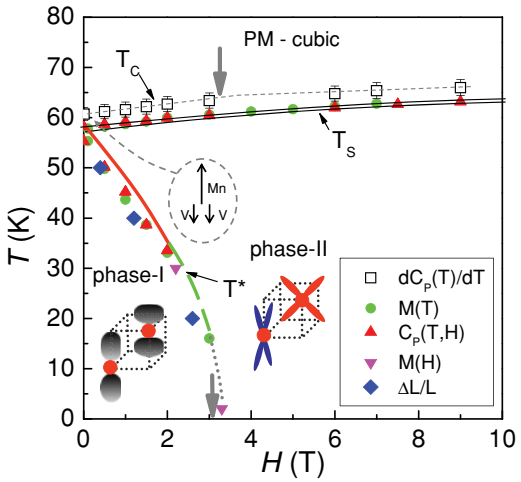

FIG. 11. (Color online) Phase diagram of MnV_2O_4 derived from the magnetization and specific-heat data. The open squares and the dashed line at ~60 K represent T_C. The solid circles, solid triangles, and the thin solid line just below T_C represent T_S. The solid circles, solid triangles, the thick solid line, and the thick dashed line below T_S represent T^*. The solid circles were obtained from the $M(T,H)$ and the solid triangles were obtained from the $C_P(T,H)$. The inverted triangles indicate the bifurcation points of the $M(H)$ isotherm. The solid diamonds denote the magnetostriction $\Delta L/L$ onset points obtained from the literature (Ref. 13). The thick arrow at ~60 K and ~3 T denote the T_S boundary slope-change point, and the thick arrow at ~0 K and ~3 T denote the specific heat γ slope-change point. The schematic picture shows the neighboring t_{2g} orbitals in a V tetrahedron.

the collinear spin-ordered state is known to change into the Yafet-Kittel-type triangular state.[14] As the magnetic field increases, the T_S also increases, which means that the magnetic field stabilizes the noncollinear ferrimagnetic spin ordering and the tetragonal lattice. As marked by the thick arrow, the slope of the T_S changes slightly at ~3 T.

As the temperature decreases further, the signature of another transition appears at T^*. T^* obtained from the specific-heat data (solid triangle) decreases drastically as the magnetic field increases (solid line). In the T-H phase diagram the T^* values form a phase boundary that divides phases I and II. Although we can observe a weak cusp near 20 K for the 3-T specific-heat data, it is too weak to be considered as a signature of T^*. Therefore, it is difficult to determine the end point of the boundary above 2 T only from $C_P(T,H)$. Instead, we observed the signature of T^* and its magnetic-field dependence also in $M(T,H)$ (solid circle), as discussed in Fig. 5. The magnetic-field dependencies of T^* obtained in different experiments are consistent with each other. Accordingly, we extend the solid line boundary up to 16 K and 3 T by using the T^* obtained from the $M(T,H)$ data (dashed line). Note that this point has some uncertainty, as indicated in Fig. 5.

It is still unclear if the phase boundary continues to the lower temperature and to the higher magnetic field. However, we found that the linear-T contribution to the specific heat (γ value at 2 K in Fig. 9) shows a change in slope at ~3 T (the downward thick arrow). Because the γ value is owing mostly to the magnetic contribution, the slope change of the γ value suggests that the low-magnetic-field state may change when crossing the phase-boundary line even at an extremely low temperature by the applied magnetic field, which suggests that the phase-boundary line approaches the zero temperature at ~3 T (dotted line).

The reorientation of the local tetragonal domain may determine the phase boundary. However, the magnetic field required for the domain reorientation at a given temperature is not relevant with the phase boundary. For example, the structural domain reorientation occurs under ~1.5 T at 56 K slightly below the T_S and above T^*, according to an x-ray scattering experiment. However, we could not observe any anomalies in the specific heat under these conditions. Therefore, it is unlikely to attribute the phase boundary to the simple domain rotation.

A NMR study suggested that the low-temperature, low-magnetic-field state is quite unusual for a simple ferrimagnet.[29] The NMR study reported that the intensity of the spectrum keeps increasing up to 4 T. The intensity increase implies short-range spin ordering or strong fluctuations between the ordered magnetic entities.[29] Such a behavior suggests that the state of phase I cannot be a long-range-ordered ferrimagnetic state. It may be a strongly fluctuating state. In addition, as shown in Fig. 5, the breakaway between the ZFC and FC magnetization is also observed in the reentrant ferromagnet, reentrant spin glass, or the cluster spin-glass materials,[17] where the long-range ordering becomes unstable owing to the fluctuations. The sharp decrease in $\chi'(f,T)$ and $\chi''(f,T)$ appears in some spin-glass materials as shown in Fig. 3, which also supports the fluctuating magnetic state for phase I.

It would be informative to review the physical properties of similar materials to identify the phases below T_S. According to the literature, $MnAl_2O_4$ shows Neél ordering below 40 K. The magnetic susceptibility shows no significant breakaway between the FC and ZFC runs. The specific-heat data show a strong peak at the Neél ordering temperature, but the signature of additional phase transition is barely observable.[6] In $MnAl_2O_4$, the only Mn ions have the spin degree of freedom. On the other hand, $MnMn_2O_4$ (or Mn_3O_4) shows a ferromagnetic transition at 42.5 K. At this temperature, a sharp peak appears in the specific-heat data, and below this temperature two small peaks appear at 40 and 35 K. Below 40 K, the breakaway between the FC and ZFC $M(T)$ curves becomes significant.[30] The crystal symmetry of $MnAl_2O_4$ and Mn_3O_4 is different from MnV_2O_4, and the Mn^{3+} ions in Mn_3O_4 have the e_g orbital degree of freedom that is different from MnV_2O_4. However, the comparison suggests that the multiple peaks in the specific heat of MnV_2O_4 are owing to the V-ion spin and the orbital contribution.

Let us look into MV_2O_4 (M = Zn, Cd). According to the literature, MV_2O_4 (M = Zn, Cd) shows two peaks at T_{C1} and at T_{C2} ($T_{C1} > T_{C2}$) in the specific-heat curve.[31] The first peak at T_{C1} is strong and the second peak at T_{C2} is weak, which is similar to that observed in MnV_2O_4. The ferrimagnetic ordering temperature, T_C, is absent in CdV_2O_4 and in ZnV_2O_4 because they are both antiferromagnetic. Therefore, we compare T_S and T^* of MnV_2O_4 with T_{C1} and T_{C2}, respectively.

The ionic radius of the M ion appears to be the control parameter for determining the T_{C1} and T_{C2} in the spinel compounds. The compound with a larger M-ion radius has a higher T_{C1} and lower T_{C2}. The ionic radius of Cd^{2+} and Zn^{2+} with a coordination number 4 is ~0.78 and 0.60 Å, respectively.[32] The T_{C1} of CdV_2O_4 is 95 K and that of ZnV_2O_4 is 55 K. The T_{C2} of CdV_2O_4 is 30 K and that of ZnV_2O_4 is 42 K. The radius of the Mn^{2+} ion with coordination number 4 is 0.65 Å, which is an intermediate of Cd^{2+} and Zn^{2+}. Therefore, we expect that T_{C1} of MnV_2O_4 would be slightly higher than 55 K. The T_{C1} of MnV_2O_4 is 58 K, which is consistent with the expectation. The consistency suggests a similar mechanism for the structural transition in the spinel compounds. In ZnV_2O_4, T_{C1} can be attributed to a cubic-tetragonal structural phase transition and the concurrent antiferro-orbital-ordering temperature.[8]

On the other hand, the T_{C2} of MnV_2O_4 is higher than expected because T_{C2} of MnV_2O_4 should be ~40 K from the trend of the spinel compounds. However, the discrepancy may not mean that the origin of T_{C2} of MnV_2O_4 is different. In the spinel lattice of MnV_2O_4, the V ions form the chain structure running along the (110) (or xy), (101) (xz), and (011) (yz) directions of the original cubic structure.[5] According to the literature, in ZnV_2O_4, first the intrachain exchange interaction stabilizes the one-dimensional antiferromagnetic state along the chains below T_{C1}, and the interchain exchange interaction stabilizes the three-dimensional antiferromagnetic state below T_{C2} as the temperature decreases.[8] According to Chung *et al.*, the interchain exchange interaction along the c axis in MnV_2O_4 appears to be relatively stronger than in ZnV_2O_4.[14] The large exchange interaction yields a higher magnetic transition temperature, which means that the discrepancy of the T_{C2} of MnV_2O_4 from the trend could be owing to the enhancement of the interchain exchange interaction strength.

In other words, the antiferromagnetic interchain exchange interaction still can be the cause of the T^* in MnV_2O_4. The antiferromagnetic ordering temperature becomes suppressed by the high magnetic field owing to the breaking of the Neél ordering.[33] The magnetic-field dependence of T^* suggests that the scenario of the antiferromagnetic interaction as a cause of the phase boundary in MnV_2O_4 is plausible.

In MnV_2O_4, the c axis becomes shorter than the a and b axes below T_S. This flattening accompanies the distortion of the VO_6 octahedra and the ordering of the V t_{2g} orbitals. One of two V electrons occupies the xy orbital at every site. The other electron has the freedom to fill one of the yz and zx orbital or both of them with partial probabilities. The xy orbital is responsible for the in-plane (or intrachain) exchange interaction and the other orbitals are responsible for the out-of-plane (or interchain) exchange interaction. X-ray and neutron scattering studies demonstrate that the space-group symmetry of MnV_2O_4 is $I4_1/a$ type, which is consistent with the picture of the alternative ordering of the yz and zx orbitals, the so-called A-type antiferro-orbital ordering.[13,14] The antiferro-orbital ordering should induce the ferromagnetic interchain exchange interaction when we count the nearest-neighbor superexchange interaction between V ions only, which is inconsistent with the argument of an antiferromagnetic interchain interaction along the c axis.[14]

However, such an inconsistency can be overcome by the orbital-fluctuation scenario. If antiferro-orbital ordering is not perfect owing to the orbital fluctuations, and if the fluctuations are not strong enough to break the static $I4_1/a$-type crystal symmetry, as Suzuki *et al.* and Chung *et al.* suggested,[13,14] then the exchange interaction should be fluctuating also. Hence, the interchain exchange interaction can have an antiferromagnetic and ferromagnetic nature, and the low-magnetic-field state can be a spin-glass-like magnetic state (phase I). The strong magnetic field suppresses the antiferromagnetic fluctuations and stabilizes the long-range-ordered ferromagnetic state. The spin-orbit coupling will also suppress the orbital fluctuations, which will lead to an antiferro-orbital-ordered state (phase II). An orbital-fluctuating state and an orbital-ordered state are schematically depicted in Fig. 11. It is also highly likely that the complicated quantum mechanical mixture of orthogonal orbitals forms an antiferro-orbital-ordered state, which can also cure the inconsistency as suggested in literature.[34,35] Further experimental studies are desirable for a concrete understanding of the orbital state.

The large magnetostriction effect is consistent with the suppression of the orbital fluctuations by the magnetic field. According to Suzuki *et al.*, the change in length ($\Delta L/L$) along the c axis increases rapidly with increasing magnetic field up to 2.5 T at 20 K, but the slope of the increase changes drastically above 2.5 T.[13] A significant change in slope occurs at 1.2 T for the 40-K isothermal $\Delta L/L$ curve, and the change in slope occurs at 0.4 T for the 50-K curve.[13] The magnetic fields of the slope-change points were marked in Fig. 11 (solid diamond), and the slope-changes points coincide with the phase boundary. The lattice with the ordered orbitals could be elongated further along the c axis than the lattice with the fluctuating orbitals. The orbital-ordered state (phase II) would require a longer unit cell length than the orbital-fluctuating state (phase I) along the c axis. Therefore, the slope-change magnetic fields of $\Delta L/L$ can coincide with the phase boundary between two orbital phases.

Furthermore, the bifurcation end points of the isothermal $M(H)$ are also on the boundary line (inverted triangles). As shown in Fig. 6, the bifurcation ends at 3.3 T in the $M(H)$ curve at 2 K, and it ends at 2.2 T in the 30-K curve. The bifurcation is reminiscent of the magnetization of the magnetic multilayer systems. In the multilayer systems, the bifurcation in the $M(H)$ curve is owing to the exchange bias between the ferromagnetic and the antiferromagnetic layers.[36] Such a layered structure does not exist in MnV_2O_4. However, the fluctuating orbitals of phase I result in an antiferromagnetic exchange interaction, which coexists with the ferromagnetic exchange interaction along the c axis. The antiferromagnetic interaction may cause the exchange bias to the ferromagnetic chains. In the spin value systems, the bifurcation ends when the external magnetic field exceeds the antiferromagnetic interaction. Analogously, the end of the bifurcation in MnV_2O_4 could be owing to the suppression of the antiferromagnetic interaction by the magnetic field.

The orbital fluctuation results in the coexistence of exchange interactions with different signs, but it does not induce a random magnetic state along the c axis in phase I. We estimated the change in entropy at the small peak as follows. By using the $C_P(T)/T$ curve at $H = 3$ T, we subtracted the other contributions to the C_P and evaluated the only contribution of C_P related to the transition. Subsequently, we calculated the change in the magnetic entropy ΔS_m by integrating the peak of $C_P(T)/T$ around T^*, where $\Delta C_P(T) = C_P(T,0) - C_P(T,3\text{ T})$. The change of the magnetic entropy is $\Delta S_m \approx 0.7$ J/mol, which is equivalent to 0.08 K_B/cell. It is only 2% of the change in entropy expected for the transition between a random spin state and a fully spin-ordered state. Therefore, a small change in the magnetic entropy suggests that the boundary represents the transition between the ordered magnetic states such as the ferromagnetic chains.

Little information is known about the magnetic state of phase II. However, a high-temperature state of phase II appears between T_S and T^* under 0 T. We guess the ground state of phase II from the high-temperature state. As shown in Fig. 3, the $M(T)$ curve between T_S and T^* is similar to that of a simple three-dimensional ferromagnet. For this temperature range, it has been known that the Mn spins are aligned along the c axis, and V spins are canted with respect to the c axis, as schematically shown in Fig. 11. A neutron-scattering study reported that the magnetic moment of Mn spins is 4.2 μ_{Bohr} and that of V spins is 1.3 μ_{Bohr}.[14] The saturation magnetic moment should be $\sim$2.9 μ_{Bohr}, if the triangular spin configuration saturates with a canting angle of 65°. At 2 K the saturation magnetic moment is almost 3 μ_{Bohr} up to 9 T, which suggests that the ground state of phase II is an ordered triangular spin state.

V. CONCLUSION

We proposed a phase diagram of a MnV_2O_4 single crystal based on an analysis of the wide-range temperature and magnetic-field dependence of the magnetic susceptibility and

specific heat. The phase diagram reveals a high-temperature paramagnetic state and a low-temperature ferrimagnetic state. The low-temperature ferrimagnetic state consists of a low-magnetic-field phase and a high-magnetic-field phase. The low-magnetic-field phase is similar to the spin-glass state. The spin-glass-like state may be owing to the competition between the ferromagnetic and the antiferromagnetic exchange interaction caused by the fluctuations of the V-ion orbitals. The high-magnetic-field state is thought to be a three-dimensional ferromagnetic state with antiferro-orbital ordering.

ACKNOWLEDGMENTS

We acknowledge G. Jackeli and S. Bayrakci for valuable discussions. K.M.-W. acknowledges the Alexander von Humboldt foundation for the support.

[1] R. Plumier and M. Sougi, Physica B **155**, 315 (1989).
[2] R. Plumier and M. Sougi, Solid State Commun. **64**, 53 (1987).
[3] K. Adachi, T. Suzuki, K. Kato, K. Osaka, M. Takata, and T. Katsufuji, Phys. Rev. Lett. **95**, 197202 (2005).
[4] Y. Yamasaki, S. Miyasaka, Y. Kaneko, J.-P. He, T. Arima, and Y. Tokura, Phys. Rev. Lett. **96**, 207204 (2006).
[5] Paolo G. Radaelli, New J. Phys. **7**, 53 (2005).
[6] N. Tristan, J. Hemberger, A. Krimmel, H. A. Krug von Nidda, V. Tsurkan, and A. Loidl, Phys. Rev. B **72**, 174404 (2005).
[7] S. Nizioł, Phys. Status Solidi A **18**, K11 (1973).
[8] S.-H. Lee D. Louca, H. Ueda, S. Park, T. J. Sato, M. Isobe, Y. Ueda, S. Rosenkranz, P. Zschack, J. Íñiguez, Y. Qiu, and R. Osborn, Phys. Rev. Lett. **93**, 156407 (2004).
[9] Y. Motome and H. Tsunetsugu, Phys. Rev. B **70**, 184427 (2004).
[10] O. Tchernyshyov, Phys. Rev. Lett. **93**, 157206 (2004).
[11] V. Hardy, Y. Breard, and C. Martin, Phys. Rev. B **78**, 024406 (2008).
[12] H. D. Zhou, J. Lu, and C. R. Wiebe, Phys. Rev. B **76**, 174403 (2007).
[13] T. Suzuki, M. Katsumura, K. Taniguchi, T. Arima, and T. Katsufuji, Phys. Rev. Lett. **98**, 127203 (2007).
[14] J.-H. Chung, J.-H. Kim, S.-H. Lee, T. J. Sato, T. Suzuki, M. Katsumura, and T. Katsufuji, Phys. Rev. B **77**, 054412 (2008).
[15] I. Yeung, R. M. Roshko, and G. Williams, Phys. Rev. B **34**, 3456 (1986).
[16] I. Nakai, J. Phys. Soc. Jpn. **64**, 588 (1995).
[17] G. G. Kenning, D. Chu, and R. Orbach, Phys. Rev. Lett. **66**, 2923 (1991).
[18] R. V. Chamberlin, M. Hardiman, L. A. Turkevich, and R. Orbach, Phys. Rev. B **25**, 6720 (1982).
[19] B. V. B. Sarkissian, J. Phys. F **11**, 2191 (1981).
[20] M. J. P. Gingras, C. V. Stager, N. P. Raju, B. D. Gaulin, and J. E. Greedan, Phys. Rev. Lett. **78**, 947 (1997).
[21] J. N. Reimers, J. E. Greedan, R. K. Kremer, E. Gmelin, and M. A. Subramanian, Phys. Rev. B **43**, 3387 (1991).
[22] N. P. Raju, E. Gmelin, and R. K. Kremer, Phys. Rev. B **46**, 5405 (1992).
[23] K. Tomiyasu, J. Fukunaga, and H. Suzuki, Phys. Rev. B **70**, 214434 (2004).
[24] D. Meschede, F. Steglich, W. Felsch, H. Maletta, and W. Zinn, Phys. Rev. Lett. **44**, 102 (1980).
[25] V. Tsurkan, M. Baran, R. Szymczak, H. Szymczak, and R. Tidecks, Physica B **296**, 301 (2001).
[26] R. Wendler, C. Pappa, C. Eckart, and K. Baberschke, J. Phys. C **20**, 2759 (1987).
[27] J. Mydosh, *Spin Glass: An Experimental Introduction* (Taylor & Francis, London, 1993).
[28] E. S. R. Gopal, *Specific Heats at Low Temperatures* (Plenum, New York, 1966).
[29] S.-H. Baek, K.-Y. Choi, A. P. Reyes, P. L. Kuhns, N. J. Curro, V. Ramanchandran, N. S. Dalal, H. D. Zhou, and C. R. Wiebe, J. Phys. Condens. Matter **20**, 13518 (2007).
[30] R. Tackett, G. Lawes, B. C. Melot, M. Grossman, E. S. Toberer, and R. Seshadri, Phys. Rev. B **76**, 024409 (2007).
[31] A. N. Vasiliev, M. M. Markina, M. Isobe, and Y. Ueda, J. Magn. Magn. Mater. **300**, e375 (2006).
[32] R. D. Shannon, Acta Crystallogr. Sect. A **32**, 751 (1976).
[33] A. H. Morrish, *The Physical Principles of Magnetism* (Wiley, New York, 1965).
[34] S. H. Baek, N. J. Curro, K. Y. Choi, A. P. Reyes, P. L. Kuhns, H. D. Zhou, and C. R. Wiebe, Phys. Rev. B **80**, 140406 (2009).
[35] S. Sarkar, T. Maitra, R. Valenti, and T. Saha-Dasgupta, Phys. Rev. Lett. **102**, 216405 (2009).
[36] J. Nogu and I. K. Schuller, J. Magn. Magn. Mater. **192**, 203 (1999).